Int. J. Automotive Composites, Vol. 3, Nos. 2/3/4, 2017

Elasto-plastic response of graphene nanoplatelets reinforced polymer composite materials

Wiyao Azoti* and Ahmed Elmarakbi
Faculty of Engineering and Advanced Manufacturing,
University of Sunderland,
SR6 0DD, UK
Email: wiyao.azoti@sunderland.ac.uk
Email: ahmed.elmarakbi@sunderland.ac.uk
*Corresponding author

Hisham El-Hage and Mustafa Elkady
Lebanese International University Beirut,
P.O. Box 146404, Mouseitbeh, Mazraa, Lebanon
Email: hisham.elhage@liu.edu.lb
Email: mostafa.kady@liu.edu.lb

Abstract: In this paper, graphene nanoplatelets GNPs have been used as continuum phases for polymer composite materials. For such a purpose, a multi-scale strategy embedding the constitutive law of each material phase is accounted for to obtain the effective properties. The elasto-plastic response is established in the framework of the J_2 plasticity. An expression of the algorithmic tangent operator for each phase is obtained and used as uniform modulus for homogenisation purpose. Using the Mori-Tanaka scheme, the effective non-linear behaviour is predicted for micro-parameters such as the aspect ratio and volume fractions. The results are compared to available experimental data as well as modelling from the literature. They show an enhancement of the equivalent macro stress-strain response with respect to low aspect ratio corresponding to platelet-like inclusions. Also, the volume fraction is seen to improve the composite response.

Keywords: Graphene composites, Mori-Tanaka scheme, Elasto-plasticity, Effective properties.

Biographical notes: Wiyao Azoti obtained his PhD in Materials science from University of Lorraine, France. His research activities lie in the framework of mechanics of materials from mean-field homogenisation and multi-scale modelling of composite materials to analytical and computational aspects of solid mechanics.

Ahmed Elmarakbi obtained his PhD in Mechanical Engineering from University of Toronto, Canada (2004). After a couple of successful postdoctoral fellowships in Canada and Japan, he moved to the UoS, UK in 2007, where he is, currently, a Professor of Automotive Engineering. His researchinterests lie in the area of energy-efficient and safe vehicles (EESVs) including low carbon vehicles, advanced composite materials, including graphene, for automotive applications.

Hisham El-Hage is a Professor in the Department of Mechanical Engineering at the Lebanese International University. He received his BASc Honours in Civil Engineering, MASc and PhD in Mechanical Engineering from the University

of Windsor, Windsor, ON, Canada. He worked for reputable international corporations. His last industrial assignment was at Msx International, Dearborn MI, USA, where crashworthiness for automotive applications were performed (Ford Motor Company, Isuzu).

Mustafa Elkady is an Assistant Professor in the Department of Mechanical Engineering at the Lebanese International University. He received his BE in Automotive Engineering in 1998 from the Ain Shams University, Faculty of Engineering, Cairo, Egypt, his MS in spark ignition engines control in 2004, and his PhD in Vehicle Dynamics Control Systems and Vehicle Crashes in 2012 from University of Sunderland, Sunderland, UK.

This paper is a revised and expanded version of a paper entitled 'Multi scale modelling of graphene platelets reinforced polymer matrix composite materials' presented at International Conference on Automotive Composites, Lisbon, 22–24 September, 2016.

1 Introduction

The current growing pressure on automotive manufacturers to have strong decarbonisation targets and to reduce annual CO_2 emissions has led to the development of advanced composite materials (ACM) that offer substantial weight reduction while improving strength. The automotive industry, as one of the largest and critical sectors of the global economy, is widely viewed as an area of the greatest volume use for ACM in the future for the production of light vehicles. Therefore, the design of the new generation of vehicles should be developed aiming for individual mobility whilst also retaining safety, environmental friendliness and affordability as reported by Kopp et al. (2012). However, the use of ACM in structural vehicle body applications has been far less extensive as described by Fuchs et al. (2008). In addition, Joost (2012) reported significant hurdles with respect to the improved performance, manufacturability, cost, and modelling of ACM. As a consequence, considerable materials science effort and new material discovery need to be developed to overcome these hurdles.

Graphene is at the centre of an ever-growing academic and industrial interests because it can produce a dramatic improvement in mechanical properties at low filler contents Kuilla et al. (2010). Indeed, Young et al. (2012) reported that one of the most immediate applications for graphene resides in composite materials. Therefore, to take a full advantage of its properties, integration of individual graphene sheets in polymer matrices is important. Exceptional physical as well as thermomechanical properties, a high surface/volume ratio and low filler content of graphene make it a promising candidate for developing the next-generation of polymer composites as shown in works by Park and Ruoff (2009), Soldano et al. (2010), or Inagaki et al. (2011). Graphene has been used to increase stiffness, toughness, thermal conductivity and viscoplastic mechanical behaviour of polymer resins by a large margin Rafiee et al. (2010), Veca et al. (2009), Xu and Gao (2010), Zhang et al. (2010), Vieira et al. (2015). However, many challenges, including the lack of constitutive material modelling for high-performance structural applications can affect the final properties and applications of graphene composites.

In this work, it is aimed to address the constitutive modelling of graphene-based polymer composite materials for understanding its contribution to the enhancement of polymer matrix composites for lightweight structural applications. Graphene is considered as

platelets embedded within a rate-independent elasto-plastic matrix phase. The composite response is therefore computed under a boundary value problem by applying static or kinematic admissible loading. Mean field homogenisation scheme, for instance, the Mori-Tanaka is used to obtain the overall response of the composite.

2 Mean field homogenisation

A macroscopic homogeneous material which is heterogeneous at the micro scale is selected under a representative volume element RVE as depicted by Figure 1. The associated boundary-value problem is formulated, in the terms of uniform macro field traction vector or linear displacement fields. The RVE is assumed to be in equilibrium and its overall deformation compatible. Also, the body forces and inertia term are neglected.

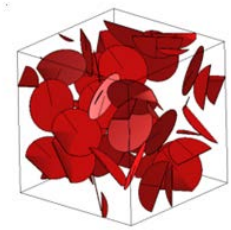

Figure 1: 3D schematics of a RVE containing platelets reinforced matrix.

These general considerations are restricted to the case of a linear constitutive law under a small transformation approximation. They can be summarised like:

$$\sigma_{ij,j} = 0 \tag{1}$$

$$\varepsilon_{ij} = \frac{1}{2}\left(u_{i,j} + u_{j,i}\right) \tag{2}$$

where σ_{ij}, ε_{ij} and u_i represent respectively the components of the stress and strain tensors and the elastic displacement. At each point r in the RVE, the local elastic constitutive law is written such as:

$$\sigma_{ij}\left(r\right) = c_{ijkl}\left(r\right)\varepsilon_{kl}\left(r\right) \tag{3}$$

The scale transition is now introduced to make the relationship between the micro scale (local) and macro scale (global) elastic properties. It consists firstly in the localisation step by the global strain tensor $\boldsymbol{A}$ such as:

$$\varepsilon_{ij}\left(r\right) = A_{ijkl}\left(r\right)E_{kl} \tag{4}$$

The second step of the scale transition is the homogenisation which employs averaging techniques to approximate the macroscopic behaviour:

$$\Sigma_{ij} = \frac{1}{V}\int_{V}\sigma_{ij}\left(r\right)dV \tag{5}$$

$$E_{ij} = \frac{1}{V}\int_V \varepsilon_{ij}(r)\,dV \qquad (6)$$

Replacing Eq. (4) in Eq. (3) and combining the result with Eq. (5), leads to the effective properties given by:

$$C_{ijkl}^{eff} = \frac{1}{V}\int_V c_{ijmn}(r)\,A_{mnkl}(r)dV \qquad (7)$$

Or in others terms

$$\boldsymbol{C}^{eff} = \sum_{I=0}^{N} f_I \boldsymbol{c}^I : \boldsymbol{A}^I \qquad (8)$$

with $\boldsymbol{c}^I$, $\boldsymbol{A}^I$, f_I the uniform stiffness tensor, the global strain concentration tensor and the volume fraction of phase I respectively. Using, the Eshelby's inclusion concept Eshelby (1957), the final expression of the global strain concentration tensor is given by an iterative procedure proposed by Vieville et al. (2006) such as:

$$\begin{cases} \boldsymbol{A}^I = \boldsymbol{a}^I : \left\langle \boldsymbol{a}^I \right\rangle^{-1} \\ \left(\boldsymbol{a}^I\right)_0 = \mathbf{I} \\ \left(\boldsymbol{a}^I\right)_{i+1} = \left(\mathbf{I} + \boldsymbol{T}^{II} : \Delta\boldsymbol{c}^I\right)^{-1} : \left(\mathbf{I} - \sum_{\substack{J=0 \\ J\neq I}}^{N} \boldsymbol{T}^{IJ} : \Delta\boldsymbol{c}^J : \left(\boldsymbol{a}^J\right)_i\right) \\ I = 0,1,2,3,.....,N \end{cases} \qquad (9)$$

where $\boldsymbol{a}^I$ states for the local strain concentration tensor and $\Delta\boldsymbol{c}^J = \boldsymbol{c}^J - \boldsymbol{c}^0$. $\boldsymbol{T}^{IJ}$ represents the interaction tensor between inclusions. In the case where the interactions between inclusions are neglected i.e $\boldsymbol{T}^{IJ} = 0$ (most of cases in the open literature), the local concentration tensor $\boldsymbol{a}^I$ reads more simple expression:

$$\boldsymbol{a}^I = \left[\mathbf{I} + \boldsymbol{T}^{II} : \Delta\boldsymbol{c}^I\right]^{-1} = \left[\mathbf{I} + \mathbf{S} : \left(\boldsymbol{c}^0\right)^{-1} : \Delta\boldsymbol{c}^I\right]^{-1} \qquad (10)$$

where $\mathbf{S}$ represents the Eshelby's tensor Eshelby (1957). Its expression depends on the aspect ratio $\alpha = c/a$ of the ellipsoidal inclusion of semi-axis (a,b,c) and the material properties of the surrounding matrix $\boldsymbol{c}^0$. Under the Mori and Tanaka (1973) assumptions, the global strain concentration tensor of the matrix is expressed as Vieville et al. (2006), Azoti et al. (2015):

$$\boldsymbol{A}^0 = \boldsymbol{a}^0 : \left\langle \boldsymbol{a}^I \right\rangle^{-1} = \left(f_0\mathbf{I} + \sum_{I=1}^{N} f_I \boldsymbol{a}^I\right)^{-1} \qquad (11)$$

leading to the effective MT properties through Eq. (8) such as:

$$\boldsymbol{C}^{MT} = \sum_{I=0}^{N} f_I \boldsymbol{c}^I \boldsymbol{A}^I = \left(f_0 \boldsymbol{c}^0 + \sum_{I=1}^{N} f_I \boldsymbol{c}^I \boldsymbol{a}^I \right) : \boldsymbol{A}^0 \tag{12}$$

3 Derivation of the non-linear tangent operators

Within the RVE, let us assume that one or more phases behave elasto-plastically. Referring to works by Doghri and Ouaar (2003) at least two tangent operators can be defined: the "continuum" (or elasto-plastic) $\boldsymbol{C}^{ep}$ tangent operator, which is derived from the rate constitutive equation, and the "consistent" (or algorithmic) $\boldsymbol{C}^{a\lg}$ tangent operator, which is solved by a discretisation in the time interval $\left[t_n,\ t_{n+1}\right]$. These tangent operators are related to the rate of the constitutive equation as follows:

$$\begin{cases} \dot{\boldsymbol{\sigma}} = \boldsymbol{C}^{ep} : \dot{\boldsymbol{\varepsilon}} \\ \delta\boldsymbol{\sigma}_{n+1} = \boldsymbol{C}^{a\lg} : \delta\boldsymbol{\varepsilon}_{n+1} \end{cases} \tag{13}$$

They are derived from the classical J_2 flow rule:

$$\begin{cases} \boldsymbol{\sigma} = \boldsymbol{C}^{el} : \left(\boldsymbol{\varepsilon} - \boldsymbol{\varepsilon}^p \right) \\ f = \sigma_{eq} - R\left(p\right) - \sigma_Y \\ \dot{\boldsymbol{\varepsilon}}^p = \dot{p}\boldsymbol{N},\ \ \boldsymbol{N} = \dfrac{\partial f}{\partial \boldsymbol{\sigma}} = \dfrac{3}{2}\dfrac{dev\left(\boldsymbol{\sigma}\right)}{\sigma_{eq}} \\ \sigma_{eq} = \left(\dfrac{3}{2}\boldsymbol{s} : \boldsymbol{s} \right)^{1/2} \end{cases} \tag{14}$$

The "continuum" (or elasto-plastic) $\boldsymbol{C}^{ep}$ tangent operator yields:

$$\begin{cases} \boldsymbol{C}^{ep} = \boldsymbol{C}^{el} - \dfrac{\left(2\mu\right)^2}{h} \boldsymbol{N} \otimes \boldsymbol{N} \\ h = 3\mu + \dfrac{dR}{dp} > 0 \end{cases} \tag{15}$$

while the "consistent" (or algorithmic) $\boldsymbol{C}^{a\lg}$ tangent operator is given by:

$$\begin{cases} \boldsymbol{C}^{a\lg} = \boldsymbol{C}^{ep} - \left(2\mu\right)^2 \Delta p \dfrac{\sigma_{eq}}{\sigma_{eq}^{tr}} \dfrac{\partial \boldsymbol{N}}{\partial \boldsymbol{\sigma}} \\ \dfrac{\partial \boldsymbol{N}}{\partial \boldsymbol{\sigma}} = \dfrac{1}{\sigma_{eq}} \dfrac{3}{2} \mathbf{I}^{dev} - \boldsymbol{N} \otimes \boldsymbol{N} \end{cases} \tag{16}$$

In equations (15) and (16), μ denotes the material shear modulus while $\boldsymbol{C}^{el}$ represents the elastic stiffness tensor and $R\left(p\right)$ is the hardening stress function with p the accumulated plastic strain. $\boldsymbol{N}$ represents the normal to the yield surface in the stress space. σ_{eq}^{tr} denotes a trial elastic predictor of σ_{eq}. $\mathbf{I}^{dev}$ stands for the deviatoric part of the fourth order symmetric identity tensor. The knowledge of internal variables such as Δp and σ_{eq}^{tr} is important for computing the algorithmic tangent operator in Eq. (16). A detailed procedure about the update of internal variables can be found in Azoti et al. (2013). $\boldsymbol{C}^{a\lg}$ will be later used to determine the overall composite behaviour using the MT scheme by Eq. (12).

4 Numerical results and discussions

The numerical algorithm for solving the overall response of the composite material is shown in Figure 2. The start point of the algorithm is the partition of strain increment $\Delta \boldsymbol{E}$ between the matrix phase and the inclusions. To this end, Voigt assumption is used to state the strain increment in the inclusions (GPL) while an average technique expresses the strain increment in the matrix (polymer). Next, the algorithmic tangent operator of each phase is computed using Eq. (16). Due to its robustness, the generalised mid-point rule Doghri and Ouaar (2003) is applied to the algorithmic tangent operator to derive the global strain concentration tensor $\boldsymbol{A}^I$. Finally, the effective properties are obtained using Eq. (12) after a convergence checking.

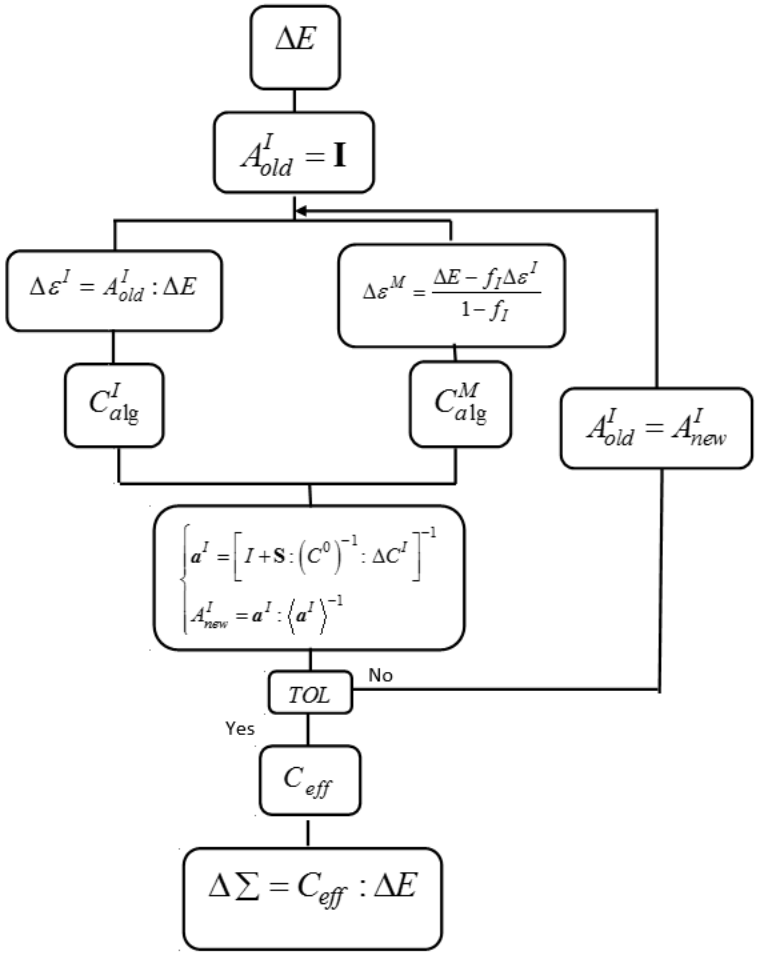

Figure 2: Numerical algorithm for the overall response of a 2-phases composite.

4.1 Model validation for a GNP/Epoxy nanocomposite

The GNP/Epoxy nanocomposite has been retained for the sake of validation due to the availability of its experimental data as well as numerical simulation. The mechanical properties of the GNPs are generally anisotropic due to their hexagonal molecular structure. Herein, GNPs were selected from works by Cho et al. (2007) through the modified Morse interatomic potential. Moreover, Elmarakbi et al. (2015) have shown that the GNPs can undergo a non-linear elastic behaviour. However, the dominant mechanical properties of the GNPs remain the in-plane behaviour which has been demonstrated to be isotropic by Cho et al. (2007). Therefore, an elastic and isotropic behaviour is selected for the GNPs. The epoxy matrix is characterised by a Young modulus and Poisson's ratio. The mechanical properties of the GNPs and the epoxy matrix are gathered in Table 1.

Table 1: Phases properties of the GNP/Epoxy composite

	GNP	**Epoxy**
Young Modulus	1.153 TPa	3.27 GPa
Poisson's ratio	0.195	0.34

Figure 3 shows the evolution of the effective Young modulus versus the aspect ratio for a GNP volume fraction of $f_I = 0.523\%$. The predictions are compared with three different experimental batches of GNP/Epoxy from works by Cho et al. (2007). The effective Young modulus varies along with the aspect ratio. A monotonic increase is observed when decreasing the values of α corresponding to platelet-like inclusions. For the studied range of the aspect ratio, a good agreement has been found between the model prediction versus both experimental data and modelling results from works by Cho et al. (2007).

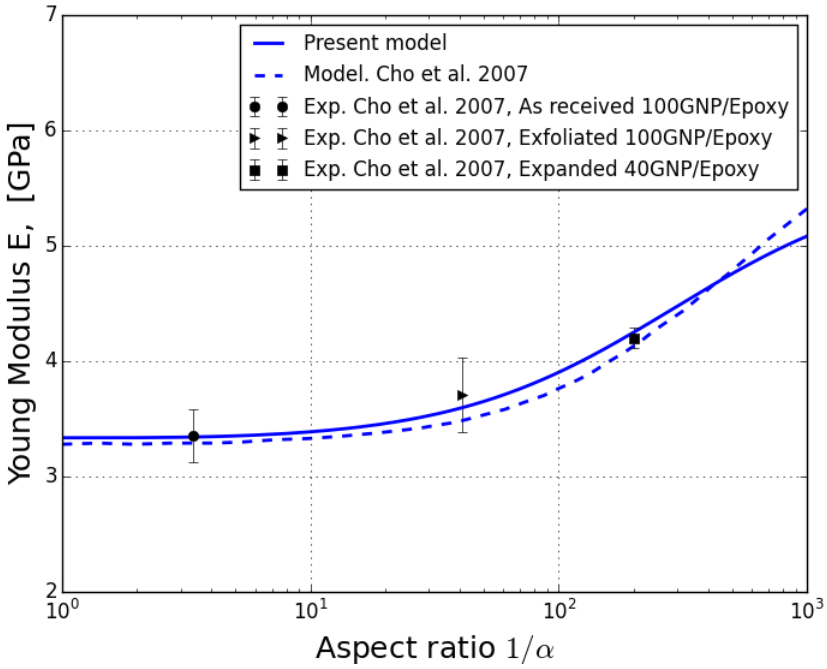

Figure 3: Effective Young modulus versus the aspect ratio for $f_I = 0.523\%$

4.2 Applications on a GNP/ PA6-B3K nanocomposite

As an application, a 2-phases composite is considered. The RVE is subjected to uniaxial as well as cyclic loadings. The load is given in terms of macro stain increment

$\Delta \boldsymbol{E} = \Delta \boldsymbol{E}.\psi$ with $\psi = e_1 \otimes e_1 - \frac{1}{2}\left[e_2 \otimes e_2 + e_3 \otimes e_3\right]$. The matrix is an elasto-plastic Polymer PA6-B3K with an isotropic hardening in power-law $R(p) = kp^m$ whereas the graphene inclusions are considered elastic. The properties of the matrix and the inclusions are reported in Table 2.

Table 2: Phases properties of a GPN/ PA6-B3K nanocomposite.

Matrix (Polymer PA6-B3K)					Inclusions (Graphene G2NAN)	
E_0	ν_0	σ_Y	k	m	E_I	ν_I
2000 MPa	0.39	60.5 MPa	63 MPa	0.4	1000 GPa	0.22

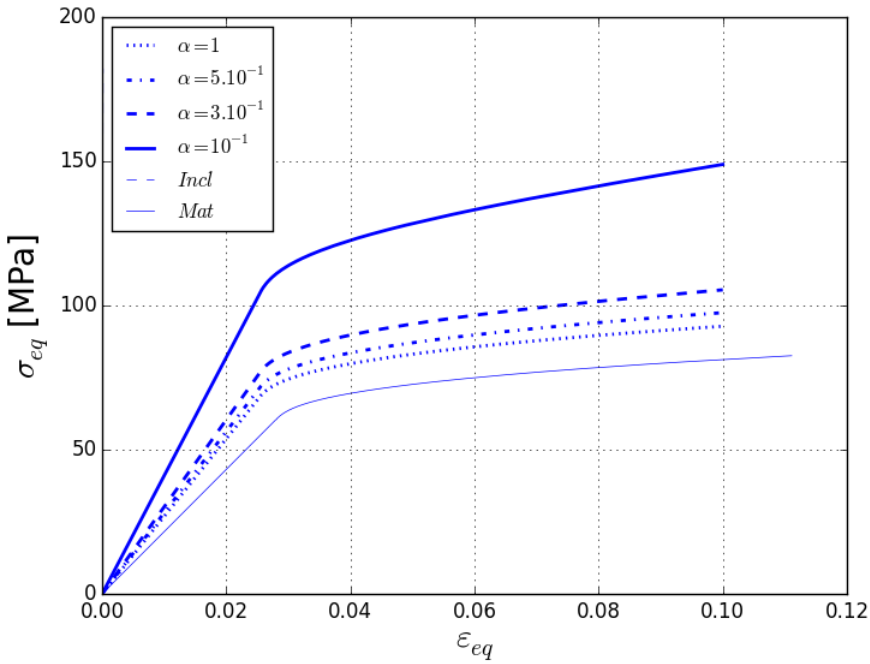

Figure 4: Aspect ratio variation for $f_I = 0.1$

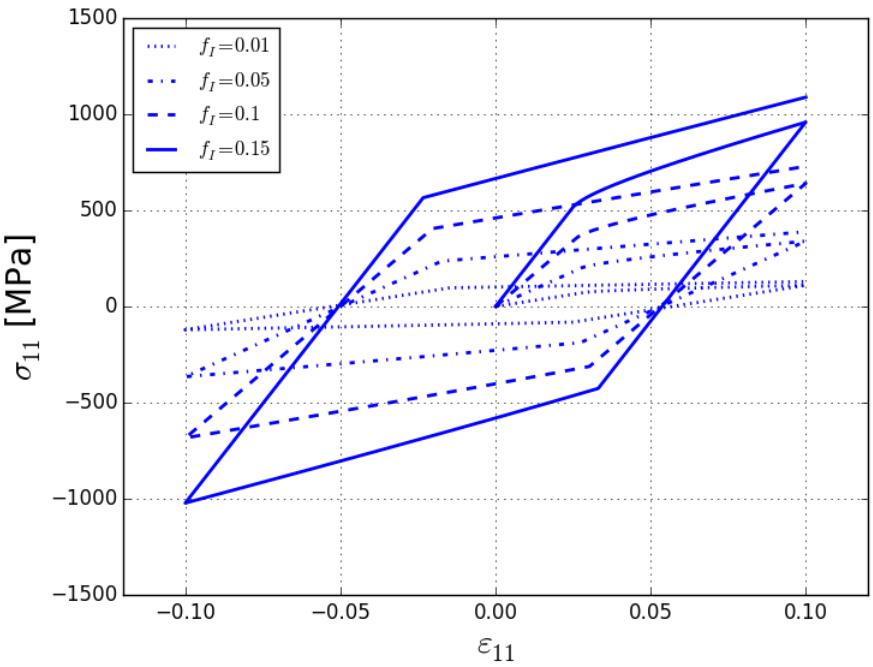

Figure 5: Cyclic loading with a volume fraction variation for $\alpha = 0.01$

Figure 4 depicts the evolution of the effective equivalent stress-strain behaviour versus the graphene aspect ratio α. For different values of α the overall response is well bonded between the responses of the matrix as well as the graphene. Also, it can be observed an increase in the overall response with respect to the decrease of α. Therefore, lower values corresponding to platelet-like inclusions show a good reinforcement character than *circular-like* inclusions i.e $\alpha = 1$. In addition, the variation of the volume fraction is analysed under a cyclic loading. The equivalent macro stress-strain response versus different volume fractions i.e $f_I = 0.01; 0.05; 0.1; 0.15$ is shown in Figure 5. The composite stress-strain response shifts towards higher stresses with the increase of the inclusions volume fraction. An enhancement of the mechanical properties is therefore noticed with the volume fraction.

5 CONCLUSION

The applicability of graphene-based polymer composite materials is made by studying the non-linear effective behaviour of a 2-phases composite. The properties of the graphene are assumed continuous elastic while an elasto-plastic polymer is considered for the matrix. The Mori-Tanaka micro-mechanics scheme derives the effective response of the composite versus the aspect ratio of the graphene sheet and its volume fraction. Predictions of the model are successfully compared with available experimental and modelling data within the literature. In addition, the results show an enhancement of the equivalent macro stress-strain response with respect to a low aspect ratio corresponding to platelet-like inclusions. The volume fraction is seen to have an improvement on the

composite response.

As further works, due to its low density and high Young modulus ($\rho_I = 1.06g/cm^3$; $E_I = 1000$ GPa) compared to its counterpart fillers like carbons fibres ($\rho_{cf} = 1.76g/cm^3$; $E_{cf} = 240$ GPa) or glass fibres ($\rho_{gf} = 2.6g/cm^3$; $E_{gf} = 85$ GPa), the GNPs are expected to demonstrate a significant enhancement in the design of high strength lightweight components and by consequence a promising approach for reducing CO_2 emissions.

Acknowledgements
The research leading to these results has received funding from the European Union Seventh Framework Programme under grant agreement No. 604391 and Horizon 2020 Programme under grant agreement No. 696656 Graphene Flagship.

References

Azoti, W., Koutsawa, Y., Tchalla, A., Makradi, A. and Belouettar, S. (2015), 'Micromechanics-based multi-site modeling of elastoplastic behavior of composite materials', *International Journal of Solids and Structures* **59**, 198 – 207.

Azoti, W., Tchalla, A., Koutsawa, Y., Makradi, A., Rauchs, G., Belouettar, S. and Zahrouni, H. (2013), 'Mean-field constitutive modeling of elasto-plastic composites using two (2) incremental formulations', *Composite Structures* **105**, 256–262.

Cho, J., Luo, J. and Daniel, I. (2007), 'Mechanical characterization of graphite/epoxy nanocomposites by multi-scale analysis', *Composites Science and Technology* **67**(1112), 2399 – 2407.

Doghri, I. and Ouaar, A. (2003), 'Homogenization of two-phase elasto-plastic composite materials and structures: Study of tangent operators, cyclic plasticity and numerical algorithms', *International Journal of Solids and Structures* **40** (7), 1681 – 1712.

Elmarakbi, A., Jianhua, W. and Azoti, W. L. (2015), 'Non-linear elastic moduli of graphene sheet-reinforced polymer composites', *International Journal of Solids and Structures* **81**, 383–392.

Eshelby, J. D. (1957), 'The determination of the elastic field of an ellipsoidal inclusion, and related problems', *Proceedings of the Royal Society of London. Series A, Mathematical and Physical Sciences* **241**(1226), 376–396.

Fuchs, E. R., Field, F. R., Roth, R. and Kirchain, R. E. (2008), 'Strategic materials selection in the automobile body: Economic opportunities for polymer composite design', *Composites Science and Technology* **68** (9), 1989 – 2002.

Inagaki, M., Kim, Y. A. and Endo, M. (2011), 'Graphene: preparation and structural perfection', *J. Mater. Chem.* **21**, 3280–3294.

Joost, W. (2012), 'Reducing vehicle weight and improving u.s. energy efficiency using integrated computational materials engineering', *JOM* **64**(9), 1032–1038.

Kopp, G., Beeh, E., Scholl, R., Kobilke, A., Strassburger, P. and Krieschera, M. (2012), 'New lightweight structures for advanced automotive vehicles-safe and modular', *Procedia - Social and Behavioral Sciences* **48**(0), 350 – 362.

Kuilla, T., Bhadra, S., Yao, D., Kim, N. H., Bose, S. and Lee, J. H. (2010), 'Recent advances in graphene based polymer composites', *Progress in Polymer Science* **35**(11), 1350 – 1375.

Mori, T. and Tanaka, K. (1973), 'Average stress in matrix and average elastic energy of materials with misfitting inclusions', *Acta Metallurgica* **21**(5), 571 – 574.

Park, S. and Ruoff, R. S. (2009), 'Chemical methods for the production of graphenes', *Nat Nano* **4**(4), 217–224.

Rafiee, M. A., Rafiee, J., Srivastava, I., Wang, Z., Song, H., Yu, Z.-Z. and Koratkar, N. (2010), 'Fracture and fatigue in graphene nanocomposites', *Small* **6**(2), 179–183.

Soldano, C., Mahmood, A. and Dujardin, E. (2010), 'Production, properties and potential of graphene', *Carbon* **48**(8), 2127 – 2150.

Veca, L. M., Meziani, M. J., Wang, W., Wang, X., Lu, F., Zhang, P., Lin, Y., Fee, R., Connell, J. W. and Sun, Y.-P. (2009), 'Carbon nanosheets for polymeric nanocomposites with high thermal conductivity', *Advanced Materials* **21**(20), 2088–2092.

Vieira, A., Pinto, V. C., Pinto, A. and Magalhães, F. D. (2015), 'Viscoplastic model analysis about the influence of graphene reinforcement in poly (lactic acid) time-dependent mechanical behaviour', *Int. J. of Automotive Composites* **Vol.1**(No.2/3), pp.244 – 257.

Vieville, P., Bonnet, A. S. and Lipinski, P. (2006), 'Modelling effective properties of composite materials using the inclusion concept. general considerations', *Arch. Mech.* **58**(3), 207–239.

Xu, Z. and Gao, C. (2010), 'In situ polymerization approach to graphene-reinforced nylon-6 composites', *Macromolecules* **43**(16), 6716–6723.

Young, R. J., Kinloch, I. A., Gong, L. and Novoselov, K. S. (2012), 'The mechanics of graphene nanocomposites: A review', *Composites Science and Technology* **72**(12), 1459 – 1476.

Zhang, W. L., Park, B. J. and Choi, H. J. (2010), 'Colloidal graphene oxide/polyaniline nanocomposite and its electrorheology', *Chem. Commun.* **46**, 5596–5598.